



Contents lists available at ScienceDirect

Journal of Quantitative Spectroscopy and Radiative Transfer

journal homepage: www.elsevier.com/locate/jqsrt

Contributions of argon, nitrogen, and oxygen to air broadening in the oxygen A-band

Leah E. Stevenson^a, Joshua L. Laughner^b, Mitchio Okumura^a, Joseph T. Hodges^c, Erin M. Adkins^{c,*}^a Division of Chemistry and Chemical Engineering, California Institute of Technology, Pasadena, CA, USA^b NASA Jet Propulsion Laboratory, California Institute of Technology, Pasadena, CA, USA^c Material Measurement Laboratory, National Institute of Standards and Technology, Gaithersburg, MD, USA

ARTICLE INFO

Keywords:

Oxygen
Line-shape parameters
Cavity ring-down spectroscopy
Remote sensing

ABSTRACT

The oxygen (O₂) A-band is used to determine the airmass in ground- and space-based remote sensing measurements because O₂ is well-mixed in the Earth's atmosphere and its column-integrated amount fraction on a dry-gas basis is nearly constant. Because biases in the retrieved airmass propagate to measurements of target species, low-uncertainty spectroscopic parameters are essential for increasingly precise and accurate greenhouse gas measurements. However, laboratory measurements and atmospheric retrievals of this O₂ band typically neglect the line-shape effects caused by collisions with argon (Ar), which comprises 0.934 % by volume of the Earth's atmosphere. To quantify the contribution of Ar to O₂ A-band air-broadening line-shape parameters, we measured pressure broadening and shifting parameters for ten high *J* lines in the P-branch of this band. These data were acquired in the laboratory over a range of pressures and nitrogen (N₂), O₂, and Ar amount fractions using cavity ring-down spectroscopy. Respective line-shape parameters for these collisional partners were determined with a multi-spectrum fitting algorithm. These results were combined with literature data to provide an empirical model for the rotational dependencies of the broadening and shifting parameters by each collisional partner. Incorporating these results into analyses of atmospheric column-integrated solar absorption spectra in the O₂ A-band shows that the neglect of Ar can lead to a small but potentially relevant systematic bias in surface pressure retrievals and a slight increase in the fit residuals of atmospheric spectra.

1. Introduction

The oxygen (O₂) A-band ($b^1\Sigma_g^+ \leftarrow X^3\Sigma_g^-(0,0)$), centered at a wavelength of 762 nm (13 123 cm⁻¹), has been used extensively in ground- and space-based remote sensing [1–5]. Because the oxygen mixing ratio in Earth's atmosphere is constant and uniform, this band has been used to characterize the atmospheric optical path to retrieve trace gas abundances [2], surface pressure [6], and aerosol and cloud properties [7–9]. Satellite missions designed to measure greenhouse gas concentrations – including JAXA's Greenhouse Gas Observing Satellite (GOSAT) [2], NASA's Orbiting Carbon Observatory-2 (OCO-2) [3] and Orbiting Carbon Observatory-3 (OCO-3) [4], and China's TanSat [5] – require high-quality O₂ spectroscopic reference data for accurate target molecule retrievals. For example, OCO-2 requires knowledge of O₂ A-band airmass retrievals to better than its overall uncertainty goal of 1 ppm column-averaged carbon dioxide amount fraction (~0.25 %) [10].

Numerous laboratory and theoretical studies have focused on improving the accuracy of O₂ A-band spectroscopic models in support of atmospheric missions [11–23]. These efforts have included highly sensitive laboratory techniques [14–16], assessment of beyond-Voigt line profiles [12,13,17], multi-spectrum fits of data from multiple sources [18,19], and the characterization of collisional effects like line mixing and collision-induced absorption [18–21]. Incorporation of these improvements has been shown to reduce residuals and surface pressure biases in OCO-2 retrievals. However, ground-based and satellite analyses show persistent systematic residuals in the O₂ A-band such that spectroscopic uncertainty remains a significant contributor to total uncertainty in atmospheric retrievals [24,25].

Spectroscopic line-shape studies in the O₂ A-band have focused on the collisional effects of oxygen and nitrogen (N₂) [11–19,22,23] because they are the primary components of the terrestrial atmosphere. Argon (Ar) and water vapor, which account for 0.934 % [26] and 0–5 %

* Corresponding author.

E-mail address: erin.adkins@nist.gov (E.M. Adkins).<https://doi.org/10.1016/j.jqsrt.2025.109480>

Received 31 January 2025; Received in revised form 10 April 2025; Accepted 15 April 2025

Available online 16 April 2025

0022-4073/Published by Elsevier Ltd.

[27] by volume of Earth's atmosphere, respectively, are the next most abundant components. Vess et al. [28] and Drouin et al. [29] investigated pressure broadening by water because atmospheric water vapor varies temporally and spatially and can therefore nonuniformly bias retrievals. Because the Ar amount fraction in the atmosphere is $<1\%$ and nearly constant, bias caused by neglecting this species in atmospheric retrievals is expected to be small. Consequently, there are few literature measurements of broadening and shifting of O₂ A-band lines by Ar.

Pope, Wolf, and Perram reported pressure broadening parameters for the noble gases in the O₂ A-band using Fourier-transform spectroscopy (FTS) [30]. They reported that collisional broadening by Ar [30] was smaller than that of O₂ or N₂ [31]. However, these spectra were only analyzed with a Voigt line profile, and the uncertainties in the measurements were large. Additionally, the Ar pressure shifts were not reported. Recent work by Klemm et al. studied Ar collisional broadening in the 1.27 μm O₂ band to compare air pressure broadening parameters reported in the literature from measurements made with synthetic- (O₂ and N₂ only) and whole- (natural) air [32]. This work found that the ratio of air to Ar collisional broadening parameters spanned from about 1.1 to 1.5 over the transitions studied.

Line-shape effects caused by collisions with Ar, particularly pressure broadening parameters, have been measured for other gases of atmospheric interest. Foreign-broadening parameters for Ar in several infrared carbon dioxide bands are generally smaller than those of O₂ or N₂ [33,34]. Experiments by Nara et al. [35], Long et al. [36], and Brewer et al. [37] suggest that failing to account for Ar pressure broadening effects in calculating air-broadening parameters can bias carbon dioxide amount fraction measurements made with commercial cavity ring-down instruments. Similarly, biases from background Ar, attributed to pressure broadening effects, have been reported for nitrous oxide by Kelley et al. [38] and for water isotopologues by Johnson and Rella [39]. To reduce such potential biases, whole-air standards with Ar are recommended for calibrating spectroscopic instruments.

In the remainder of this article, we quantify the magnitude of Ar line-shape effects in the O₂ A-band. We report line-shape parameters of ten high J transitions in the P-branch measured with frequency-agile, rapid scanning (FARS) cavity ring-down spectroscopy (CRDS) [40–42] over a range of pressures and Ar amount fractions. We analyze the data with a multi-spectrum fitting approach [43] to simultaneously determine O₂, N₂, and Ar parameters of pressure broadening and pressure shifting, as well as the air narrowing parameters for these transitions. Finally, we report numerical simulations and atmospheric spectra analyses to estimate the potential bias incurred by neglecting Ar broadening in atmospheric air mass retrievals based on O₂ A-band spectra.

2. Methods

2.1. Instrument

Measurements were made using a custom room-temperature FARS-CRDS spectrometer located at the National Institute of Standards and Technology (NIST) in Gaithersburg, Maryland, USA, which has been previously described in the literature [42]. This FARS-CRDS system uses a servo incorporating a high-precision wavelength meter to stabilize the probe laser frequency [41], while an electro-optic modulator generates a tunable first-order sideband resonant with successive longitudinal modes of the optical cavity [40]. This technique enables rapid cavity free spectral range (FSR) stepwise scanning over ~ 20 GHz frequency segments that can be combined to achieve broad spectral coverage. The resulting CRDS decay signals are sampled by a metrology-grade digitizer [44] and range from 4.3 μs to 11.1 μs with a typical relative standard deviation of about 0.05%. Each spectral data point is the average of 200 decays acquired at an acquisition rate of ~ 430 Hz.

A transmission lock to an I₂-stabilized HeNe reference laser (long-term frequency drift of about 10 kHz) was used to actively stabilize the

cavity length and, consequently, the frequency detuning axis [45] corresponding to integer multiples of the ring-down cavity FSR. This laser also served as a calibration reference for the wavelength meter, providing accurate (30 MHz standard uncertainty) laser frequencies for unambiguous selection of transitions and precise (1.4 MHz) measurements of laser frequencies resonant with the ring-down cavity used to determine the empty-cavity FSR, $\nu_{FSR,0} = 198.8624(1)$ MHz. For each sample pressure and temperature, $\nu_{FSR,0}$ was corrected by an amount, $\Delta\nu_{FSR}$, to account for changes in the refractive index caused by variations in gas density [46].

2.2. Sampling

In this study, we used five different gas samples with varying amount fractions of O₂, N₂, and Ar to determine the respective line-shape parameters. Table 1 summarizes the sample compositions used in this study. The gas samples included a pure O₂ sample, NIST Standard Reference Material (SRM®) synthetic air sample (SRM 2659a lot LS 71-EL-02), NIST SRM Southern Oceanic Air (SRM1721 lot 1721-A-29) [47], and 5% and 15% Ar-in-air samples previously described in Long et al. [36].

While the CRDS technique is highly sensitive and precise, its finite dynamic range limits the optical depths suitable for line-shape measurements. To enable measurements of the air-like samples outlined in Table 1 at pressures up to 133 kPa, we focused on ten relatively weak high J transitions in the P-branch of the O₂ A-band, P29Q28 to P37P37. The intensities of the measured transitions ranged from 0.04% to 1.2% of the maximum line intensity in this band. The transitions are labeled as $\Delta N N'' \Delta J J''$, where N is the rotational angular momentum quantum number and J is the total angular momentum quantum number (sum of rotational angular momentum and spin angular momentum). There are four allowed branches in the O₂ A-band: PP ($\Delta N = \Delta J = -1$), PQ ($\Delta N = -1, \Delta J = 0$), RR ($\Delta N = \Delta J = 1$), and RQ ($\Delta N = 1, \Delta J = 0$). In this work, we use the term P-branch to mean both the PP and PQ branches and the R-branch to mean both the RR and RQ branches.

The studied ten transitions were measured in five pairs of adjacent PP- and PQ-branch lines to allow for the fitting of first-order line mixing and overlap in the wings of the lines. For all but the pure oxygen sample, line pairs were recorded at eight pressures: 3.33 kPa, 6.66 kPa, 13.3 kPa, 26.7 kPa, 53.3 kPa, 80.0 kPa, 107 kPa, and 133 kPa. For a given pair, the pure oxygen spectra were collected at 1.3 kPa and then up to the highest pressure in the previous list that was within the dynamic range of the system. As a result, the number of pure oxygen sample pressures ranged from two (for the P29Q28 and P29P29 pair) to nine (for the P37Q36 and P37P37 pair). Fig. 1 shows typical spectra for the P35P35 and P35Q34 line pair for the various pressures and gas mixtures considered. Pressures

Table 1

Sample compositions with combined standard uncertainties given by the last digit in parentheses. Sample composition values and uncertainties appear as stated in the Reports of Analysis or previous publications [34,36]. The range of measured temperatures for each sample are also reported. *Trace Ar in the synthetic air sample is treated as negligible during fitting. **Purity of Pure O₂ sample is 99.997%.

Sample name	Ar diluent contribution (%)	O ₂ diluent contribution (%)	N ₂ diluent contribution (%)	Measured Temperatures (K)
Pure O ₂	0	100**	0	298.20 – 298.22
Synthetic-Air	0.0090*	20.868(28)	79.1319(106)	298.15 – 298.19
Whole-Air	0.93493(136)	20.93234 (118)	78.13273 (180)	298.04 – 298.10
5 % Ar	5.087(42)	19.8840(77)	75.029(43)	298.08 – 298.13
15 % Ar	14.98(12)	17.9961(69)	67.0239 (1200)	298.13 – 298.18

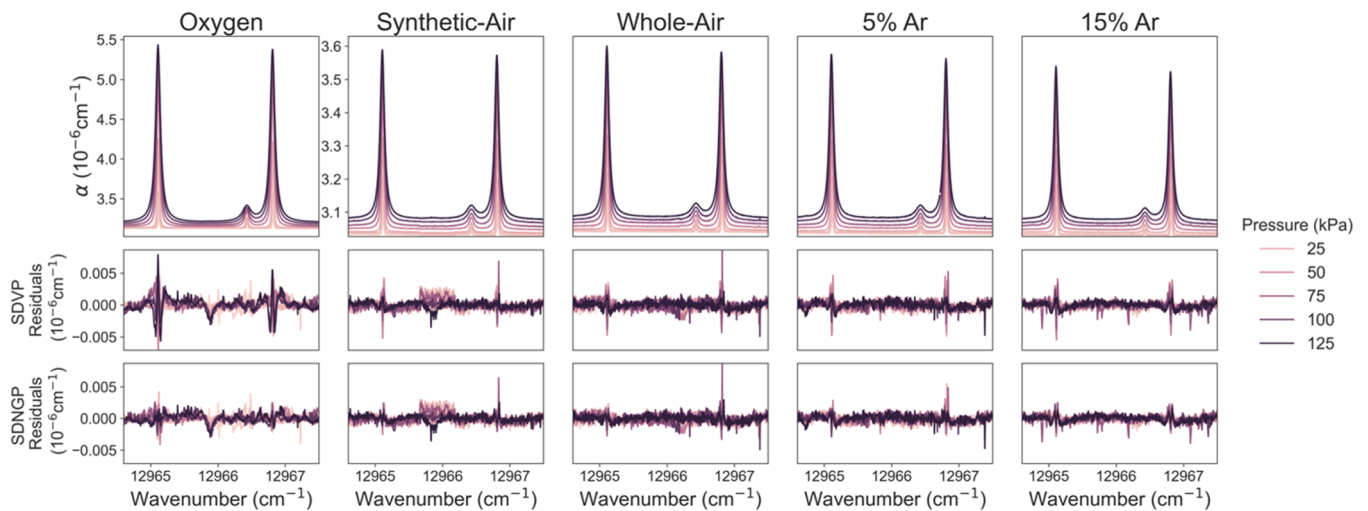


Fig. 1. Measured absorption spectra (top row) and corresponding residuals (measurement minus fit) from a multi-spectrum fit with the two different beyond-Voigt line-profiles described below: SDVP (middle row) and SDNGP (bottom row) for the P35P35 and P35Q34 lines in the O₂ A-band. The columns correspond to results for different gas samples used in the multi-spectrum analysis as outlined in Table 1, with 9 measured spectra for pure oxygen and 8 measured spectra for each of the mixtures comprising a total of 41 spectra. The average quality-of-fit-factor (QF) with the SDVP was 675 (range 76–2556), and that of the SDNGP was 836 (range 76–3361). Note the change of the y-axis scale for the oxygen spectra compared to the other samples.

were measured by a resonant silicon manometer with a full-scale range of 130 kPa and temperatures by a thermistor in good thermal contact with the cavity cell wall. Both sensors were calibrated against SI-traceable NIST transfer standards [48]. The measured temperatures for each sample are summarized in Table 1.

2.3. Multi-spectrum fitting method

We used the Multi-spectrum Analysis Tool for Spectroscopy (MATS) [43] to fit line-by-line spectral models to the measured spectra. With this multi-spectrum analysis approach, global fitted line-shape parameters can be constrained by both pressure and the amount fraction of each collisional partner. MATS uses a least-squares algorithm to minimize the residuals computed between measured spectra and those modeled using line profiles from the HITRAN application programming interfaces (HAPI) [49,50]. For each transition pair, all spectra (ranging from 34 to 41 spectra depending on available pure oxygen spectra) were fit simultaneously to extract N₂, O₂, and Ar pressure broadening and shifting parameters.

We modeled the spectrum of each line pair using Eq. (1), where $\tau(\nu)$ is the measured ring-down time constant at the cavity resonance frequency ν , c is the speed of light, $\alpha(\nu)$ is the absorption coefficient of the sample, and α_b is an empirical quadratic baseline term. The absorption coefficient is modeled through Eq. (2), where χ_{O_2} is the ¹⁶O₂ amount fraction, ρ is the ideal gas number density of the sample at the measured pressure, p_{obs} , and observed temperature T_{obs} , S_i is the line intensity, Φ_i is the area-normalized line profile, χ_j represents the amount fractions of the broadeners in the sample, and i indexes a spectral transition in the frequency range of the spectrum. All O₂ transitions in HITRAN in the spectral region were modeled in the fits as,

$$[c\tau(\nu)]^{-1} = \alpha(\nu) + \alpha_b \quad (1)$$

$$\alpha(\nu) = \chi_{O_2} \rho \sum_i S_i(T_{obs}) \Phi_i(\nu; T_{obs}, p_{obs}, \chi_j). \quad (2)$$

Fitting the measured spectra with a Voigt profile (VP) shows characteristic structure at the line core, indicating the need for fitting with beyond-Voigt line-shape profiles such as those based on the Hartmann-Tran profile (HTP) and its limiting cases. This profile is recommended for high-resolution spectroscopy, and in addition to the pressure broadening and shifting parameters, γ_0 , and δ_0 respectively, it includes

terms accounting for speed-dependent broadening, γ_2 ($a_w = \gamma_2/\gamma_0$) and shifting δ_2 ($a_s = \delta_2/\delta_0$), as well as the rate of velocity-changing collisions (Dicke narrowing), $\tilde{\nu}_{vc}$. Finally, the HTP has a correlation parameter, η , quantifying correlation between velocity- and rotation-state-changing collisions [51,52]. Here, we used two limiting cases of the HTP, the speed-dependent Nelkin-Ghatak profile (SDNGP, $\eta = 0$) and the speed-dependent Voigt profile (SDVP, $\tilde{\nu}_{vc} = 0$, $\eta = 0$). In the HTP, Dicke narrowing is based on a hard collision model, where molecular velocities before and after collisions are unrelated. Some literature data in this band were obtained using the Galatry profile (GP), which models Dicke narrowing using a soft collisional model, where it is assumed that many collisions are necessary to change the molecular velocity [52]. Analysis with the SDVP and SDNGP also modeled line mixing using the first-order Rosenkranz parameterization [53]. Line mixing was included to minimize residuals, but parameters are not reported because line mixing in the O₂ A-band is best modeled by a full matrix line mixing approach [18–20].

One significant challenge in fitting higher-order line-shape profiles to measured spectra of finite signal-to-noise is a numerical correlation between parameters, which may result in fitted values or uncertainties that are not physically meaningful [49,54]. In analysis with the SDNGP and SDVP profiles, the a_s term was set to 0 because the SNR was too low to extract physically meaningful parameters. Additionally, the a_w , $\tilde{\nu}_{vc}$, and line mixing parameters were constrained to be the same for all broadeners. This assumption was incorporated into the uncertainty quantification. The line intensities were not constrained to be equal across all spectra when fitting a given line.

Fig. 1 shows measured spectra of the P35P35 and P35Q34 lines with SDVP and SDNGP fit residuals (measurement minus fit) for the various samples. Quality-of-fit factors (QF) from the multi-spectrum fit were higher for the SDNGP (mean 836, range 76–3361) than for the SDVP (mean 675, range 76–2556), and structured residuals in the line cores were reduced with the SDNGP. The QF is defined as the baseline subtracted peak absorption coefficient divided by the standard deviation of the fit residuals. The signal-to-noise ratio (SNR) is a similar metric only considering the noise in the spectrum baseline, rather than the standard deviation in the fit residuals (mean 870, range ~75 – 3850). QFs will approach the SNR when systematic residuals from the fitting model are negligible. Spectra were also analyzed independently in multi-spectrum fits for each gas sample: on average, the QFs from these fits of single gas samples were about 7 % larger than the multi-spectrum fits that included

all spectra. This result highlights that, while these data did not have sufficiently high signal-to-noise ratios to accurately determine the higher-order line-shape parameters for each broadener, there was some sensitivity to the broadener dependence in the higher-order line-shapes.

2.4. Uncertainty analysis

Uncertainty in the reported spectroscopic parameters arises from statistical uncertainties resulting from fitting spectra with experimental noise and systematic uncertainties in measured pressure, temperature, and sample composition. Tables 2 and 3 summarize the statistical (Type A evaluation) and systematic (Type B evaluation) uncertainties [55] for each reported parameter and the combined relative uncertainties for fits with the SDNGP and SDVP, respectively.

The analysis of statistical uncertainties in the reported parameters is complicated by the numerical correlation between line-shape parameters, which can be significant for the higher-order narrowing parameters, $\tilde{\nu}_{VC}$ and a_w . As part of the multi-spectrum fitting process, MATS reports the standard error of each fitted parameter from the least-squares fit. However, this approach underestimates the statistical uncertainties because it does not account for the numerical correlation between fitted parameters. For a more conservative estimate of the statistical uncertainties, we performed Monte Carlo simulations to obtain ensembles of fitted values, following the procedure reported in Fleurbaey et al. [56]. For each pair of transitions, we used MATS to generate synthetic spectra corresponding to the sample composition, pressure, and signal-to-noise ratio of the measured spectra. Repeating this procedure multiple times with unique synthetic noise and different initial parameter guesses for each pair of transitions, we assigned the standard deviation of each ensemble to be the Monte Carlo standard uncertainty, then computed the ratio of the Monte Carlo standard uncertainty to the standard error reported by MATS for the simulations. This ratio provides a factor by which the uncertainties from a Type A evaluation can be corrected to better account for the correlation between parameters.

Systematic uncertainties in the pressure, temperature, and sample composition were evaluated for each parameter as described in Adkins et al. [34], and the results were combined in quadrature with the statistical uncertainties to calculate combined relative uncertainties. The systematic pressure uncertainty is determined by the combined uncertainty in the pressure gauge, comprising the quadrature sum involving drift in the pressure zero measurement, uncertainty in the pressure calibration, and the change in pressure across a spectrum (<10 min for spectrum collection). The temperature uncertainty for each line-shape parameter is determined by both the uncertainty in the temperature measurement (0.028 K: thermistor uncertainty, deviation across measurement, and estimated gradients) and the uncertainty in the line-shape parameter's temperature dependence, which is used to report the parameter at a reference temperature of 296 K. For the collisional broadening and pressure shifting terms, the sample composition

uncertainty is based on the composition uncertainties in the samples used in the multi-spectrum fit outlined in Table 1. For $\tilde{\nu}_{VC}$ and a_w , an air-broadening value is reported, so the uncertainty associated with the sample composition includes the estimated uncertainty in the parameter based on the difference between theoretical values for air and the composite sample composition used in this study.

3. Results and discussion

Tables 4 and 5, respectively, contain broadener-dependent SDNGP and SDVP line lists for the ten reported transitions.

3.1. Line-shape parameters

In Fig. 2, we present pressure broadening parameters, γ_0 , obtained in this study as well as literature values for the three broadeners. The results are plotted as a function of total angular momentum index m , where $m = -J'$ for the P-branch and $m = J'+1$ for the R-branch. Although fewer high-resolution measurements are available for high J transitions than at the center of the band, N_2 and O_2 broadening coefficients obtained here are within 5 % percent of those reported by Robichaud et al. [14], Havey et al. [15], Drouin et al. [18], and Payne et al. [19]. There is also reasonable agreement across the band in the literature for the γ_{0,N_2} and γ_{0,O_2} parameters. It is also worth noting that the literature data includes broadening terms determined from fits of the VP [11,31], GP [14,15], and SDVP [12,13,18,19,23], which could account for some of the variation. For each broadener, we fit a second/third-order Padé approximant to the literature and present data. For the N_2 and O_2 cases, each datum was weighted by the inverse of the square of its standard uncertainty, whereas for the Ar case, the data were not weighted because there was no overlap in m between the literature values and measurements. We refer to each fit (see Supplemental Materials for numerical results) as the empirical model, which is shown by the dashed line for each case. In the empirical models for the N_2 and O_2 cases, we excluded the VP-based results of Brown and Plymate [11] and Pope et al. [31] because their collisional broadening terms are expected to be smaller than those from higher-order profiles that account for line narrowing mechanisms. We note, however, that the Pope et al. γ_{0,O_2} data are systematically larger than those of the literature, in opposition to the expected trend. Nevertheless, we used the Pope et al. data [30] in the empirical model for Ar broadening because these results are the only Ar-broadened O_2 A-band data available in the literature. Fit residuals in the lower panel of Fig. 2 show the differences between the present measurements and literature data relative to the empirical model, where the standard deviation of the residuals (only considering data used in the empirical model development) was 4.7 % for γ_{0,N_2} , 3.4 % for γ_{0,O_2} , and 5.1 % for $\gamma_{0,Ar}$.

For the ten transitions measured in this study, the Ar pressure broadening parameters are smaller than those of O_2 and N_2 with an average ratio $\langle \gamma_{0,Ar}/\gamma_{0,O_2} \rangle = 0.49 \pm 0.06$ compared to $\langle \gamma_{0,N_2}/\gamma_{0,O_2} \rangle =$

Table 2

Uncertainty analysis for reported SDNGP parameters. All uncertainty values are expressed as relative standard uncertainties in (%). Indicated statistical (Type A evaluation) and systematic (Type B evaluation) uncertainty values are based on the distribution median of all measured transitions. Combined uncertainties reported in Table 4 are based on the line-by-line statistical and systematic uncertainties. *Parameter value determined by constrained fit with all broadeners equal across all samples. Uncertainty quantification includes deviation from nominal air component amount fractions.

Line-shape Parameter	Broadener	Type A Evaluation		Type B Evaluation			Combined
		Fit Uncertainty	Monte Carlo Expanded Uncertainty	p	T	χ	
γ_0	N_2	0.11	0.11	0.06	0.04	0.06	0.15
	O_2	0.09	0.09		0.05	0.005	0.12
	Ar	0.5	0.6		0.05	0.06	0.60
δ_0	N_2	0.2	0.2	0.05	0.06	0.20	
	O_2	0.4	0.4	0.05	0.005	0.43	
	Ar	0.6	0.6	0.06	0.06	0.62	
$\tilde{\nu}_{VC}$	Air*	2	2	0.4	2	3	
a_w	Air*	1.3	1.3	0.2	4	5	

Table 3

Uncertainty analysis for reported SDVP parameters. All uncertainty values are expressed as relative standard uncertainties in (%). Indicated statistical (Type A evaluation) and systematic (Type B evaluation) values are based on the distribution median of all measured transitions. Combined uncertainties reported in Table 5 are based on the line-by-line statistical and systematic uncertainties. *Parameter value determined by constrained fit with all broadeners equal across all samples. Uncertainty quantification includes deviation from nominal air component amount fractions.

Line-shape Parameter	Broadener	Type A Evaluation		Type B Evaluation			Combined
		Fit Uncertainty	Monte Carlo Expanded Uncertainty	p	T	χ	
γ_0	N ₂	0.13	0.13	0.06	0.05	0.06	0.16
	O ₂	0.09	0.09		0.05	0.005	0.12
	Ar	0.8	0.8		0.05	0.06	0.8
δ_0	N ₂	0.2	0.2		0.05	0.06	0.2
	O ₂	0.4	0.4		0.05	0.005	0.4
	Ar	0.7	0.7		0.06	0.06	0.7
a_w	Air*	0.3	0.4		0.2	4	4

Table 4

Measured SDNGP parameters. Values in parentheses are combined statistical and systematic uncertainties in the last reported digit. Units are cm⁻¹ atm⁻¹ (1 cm⁻¹ atm⁻¹ = 0.295 872 15 MHz/Pa) for γ_0 , δ_0 , and $\bar{\nu}_{VC}$; a_w is dimensionless. Collisional broadening and shifting parameters are reported for N₂, O₂, and Ar broadeners, while a_w and $\bar{\nu}_{VC}$ are reported for air broadening.

Line	m	$\gamma_{0,N2}$	$\gamma_{0,O2}$	$\gamma_{0,Ar}$	$\delta_{0,N2}$	$\delta_{0,O2}$	$\delta_{0,Ar}$	$a_{w,air}$	$\bar{\nu}_{VC,air}$
P37P37	-37	0.02450(4)	0.03017(4)	0.01307(33)	-0.01075(2)	-0.00739(1)	-0.00933(20)	0.111(6)	0.0069(3)
P37Q36	-36	0.02444(5)	0.02998(4)	0.01213(32)	-0.01071(3)	-0.00688(2)	-0.00981(22)	0.108(6)	0.0063(3)
P35P35	-35	0.02649(3)	0.03153(3)	0.01414(15)	-0.01060(1)	-0.00732(1)	-0.00964(9)	0.109(5)	0.0061(2)
P35Q34	-34	0.02672(3)	0.03145(3)	0.01447(17)	-0.01051(1)	-0.00678(1)	-0.00951(10)	0.117(5)	0.0050(2)
P33P33	-33	0.02873(3)	0.03356(4)	0.01622(8)	-0.01029(1)	-0.00726(3)	-0.00946(5)	0.134(6)	0.0043(2)
P33Q32	-32	0.02898(3)	0.03349(4)	0.01641(10)	-0.01031(1)	-0.00651(3)	-0.00937(5)	0.140(6)	0.0034(1)
P31P31	-31	0.03090(4)	0.03540(10)	0.01799(4)	-0.01036(2)	-0.00620(7)	-0.00965(3)	0.121(5)	0.0055(2)
P31Q30	-30	0.03063(5)	0.03546(13)	0.01794(11)	-0.01014(2)	-0.00613(8)	-0.00934(6)	0.117(5)	0.0050(2)
P29P29	-29	0.03320(7)	0.03676(25)	0.02053(6)	-0.01025(5)	-0.00523(17)	-0.00966(3)	0.076(4)	0.0075(2)
P29Q28	-28	0.03355(8)	0.03608(26)	0.02021(6)	-0.00986(4)	-0.00585(16)	-0.00973(3)	0.083(4)	0.0061(2)

Table 5

Measured SDVP parameters. Values in parentheses are combined statistical and systematic uncertainties in the last reported digit. Units are cm⁻¹ atm⁻¹ (1 cm⁻¹ atm⁻¹ = 0.295 872 15 MHz/Pa) for γ_0 and δ_0 ; a_w is dimensionless. Collisional broadening and shifting parameters are reported for N₂, O₂, and Ar broadeners, while a_w is reported for air broadening.

Line	m	$\gamma_{0,N2}$	$\gamma_{0,O2}$	$\gamma_{0,Ar}$	$\delta_{0,N2}$	$\delta_{0,O2}$	$\delta_{0,Ar}$	$a_{w,air}$
P37P37	-37	0.02472(4)	0.03065(3)	0.01277(38)	-0.01074(3)	-0.00738(1)	-0.00932(20)	0.168(7)
P37Q36	-36	0.02466(5)	0.03043(3)	0.01178(38)	-0.01071(3)	-0.00687(2)	-0.00983(21)	0.163(7)
P35P35	-35	0.02672(3)	0.03195(3)	0.01390(18)	-0.01060(2)	-0.00732(1)	-0.00963(11)	0.159(7)
P35Q34	-34	0.02694(3)	0.03181(3)	0.01430(18)	-0.01050(2)	-0.00677(1)	-0.00950(11)	0.157(7)
P33P33	-33	0.02931(3)	0.03343(4)	0.01624(9)	-0.01029(1)	-0.00727(3)	-0.00946(5)	0.176(8)
P33Q32	-32	0.02943(3)	0.03338(4)	0.01642(10)	-0.01031(1)	-0.00649(3)	-0.00934(6)	0.173(8)
P31P31	-31	0.03171(5)	0.03453(13)	0.01800(6)	-0.01034(2)	-0.00615(8)	-0.00963(3)	0.166(7)
P31Q30	-30	0.03175(7)	0.03481(18)	0.01783(16)	-0.01012(4)	-0.00732(12)	-0.00966(8)	0.168(7)
P29P29	-29	0.03404(11)	0.03564(39)	0.02103(7)	-0.01024(5)	-0.00521(21)	-0.00967(4)	0.141(6)
P29Q28	-28	0.03428(10)	0.03514(37)	0.02046(8)	-0.00985(6)	-0.00590(21)	-0.00963(4)	0.139(6)

0.87 ± 0.05 (uncertainty represents the standard deviation over the measured lines). However, using the present empirical models and including transitions up to $J'' = 40$, we obtain $\langle \gamma_{0,Ar} / \gamma_{0,O2} \rangle = 0.69 \pm 0.19$ and $\langle \gamma_{0,N2} / \gamma_{0,O2} \rangle = 0.94 \pm 0.07$. Over the same range of J for broadening by water vapor, we find that $\langle \gamma_{0,H2O} / \gamma_{0,O2} \rangle = 1.05 \pm 0.06$ [27,57]. While water vapor broadening needs to be included in the atmospheric spectroscopic models because of its geophysical, altitudinal, and temporal variation, the difference from $\gamma_{0,N2}$ is larger for $\gamma_{0,Ar}$ than for $\gamma_{0,H2O}$. Therefore, because the amount fraction of Ar in the atmosphere is constant and nearly equal to 1 %, systematic bias in atmospheric retrievals might occur when using collisional broadening parameters based on laboratory measurements made with Ar-free synthetic air (N₂ and O₂ only).

In Fig. 3, we compare the m -dependence of present pressure shifting parameters, δ_0 , for each broadener to literature values from Brown and Plymate [11], Predoi-Cross et al. [12,13], Robichaud et al. [14], Drouin et al. [18], Payne et al. [19], Lunny [22], and Sung [23]. Most notably, there is a much more significant discrepancy in the literature between pressure shifting coefficients than between those of pressure

broadening. For pressure shifting by N₂, the data from Brown and Plymate [11] and Predoi-Cross et al. [12] are displaced from the current data and those of Robichaud et al. [14], Drouin et al. [18], Payne et al. [19], Lunny [22], and Sung [23]. For O₂, the $\delta_{0,O2}$ values reported by Lunny [22], Brown and Plymate [11], Predoi-Cross et al. [13], and Sung [23] are clustered, exhibiting an offset with respect to those of Drouin et al. [18] and Payne et al. [19]. Additionally, the results of Robichaud et al. [14] appear to be outliers compared to all other literature data and the present measurements. Unlike in the case of $\delta_{0,N2}$, the present measurements of $\delta_{0,O2}$ do not clearly agree in magnitude with one of two literature data groupings. Because the Payne et al. work [19] is the next iteration of the Drouin et al. O₂ A-band spectroscopic model [18], agreement between these values is expected. However, the line list of Sung [23] is a reanalysis of the FTS spectra included in the Drouin and Payne data set and four additional FTS spectra. The Sung [23] O₂ pressure shifts are slightly larger than other literature data but more consistent with other literature data than the related Drouin [18] and Payne [19] O₂ pressure shift values.

For the N₂ and O₂ pressure shifts, we fit first/second-order Padé

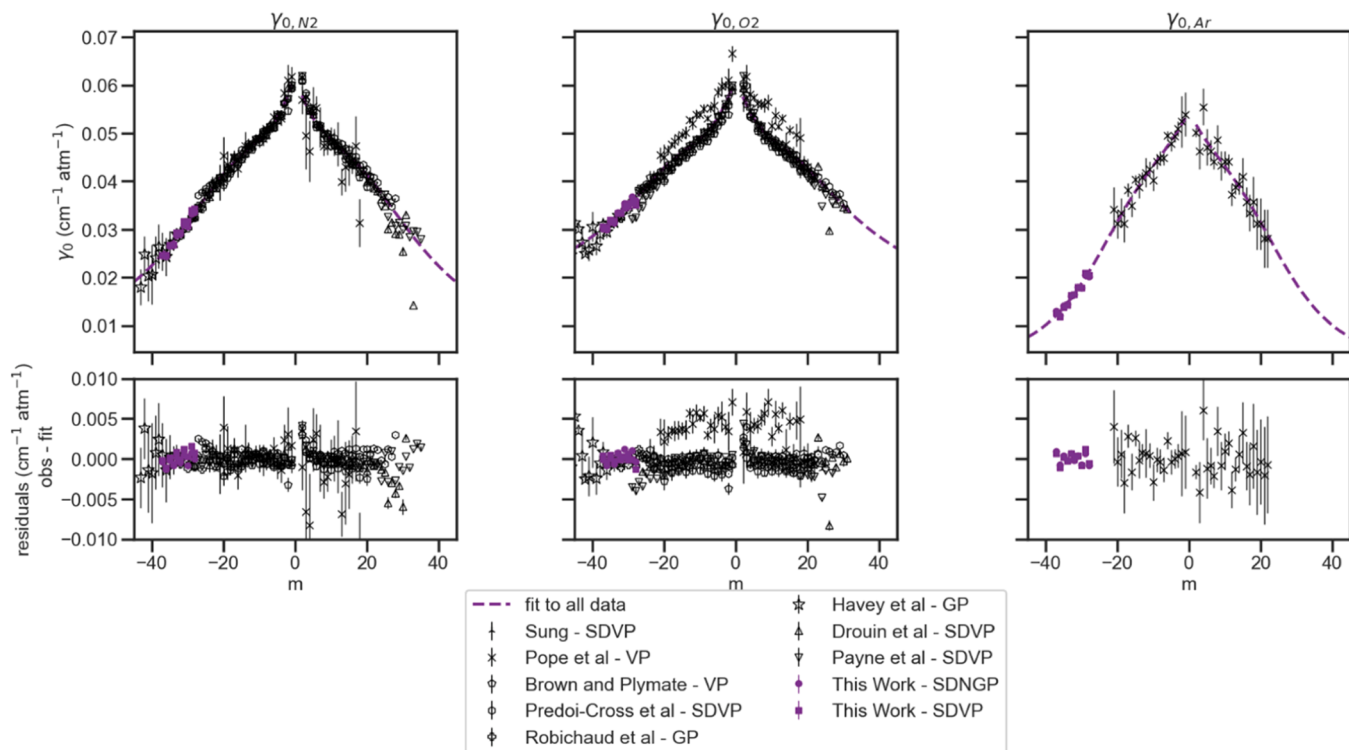


Fig. 2. Comparison of N₂, O₂, and Ar pressure broadening coefficients reported here and in the literature. Error bars represent the combined standard uncertainty in the fitted parameters for the current measurements and reported uncertainties for literature values.

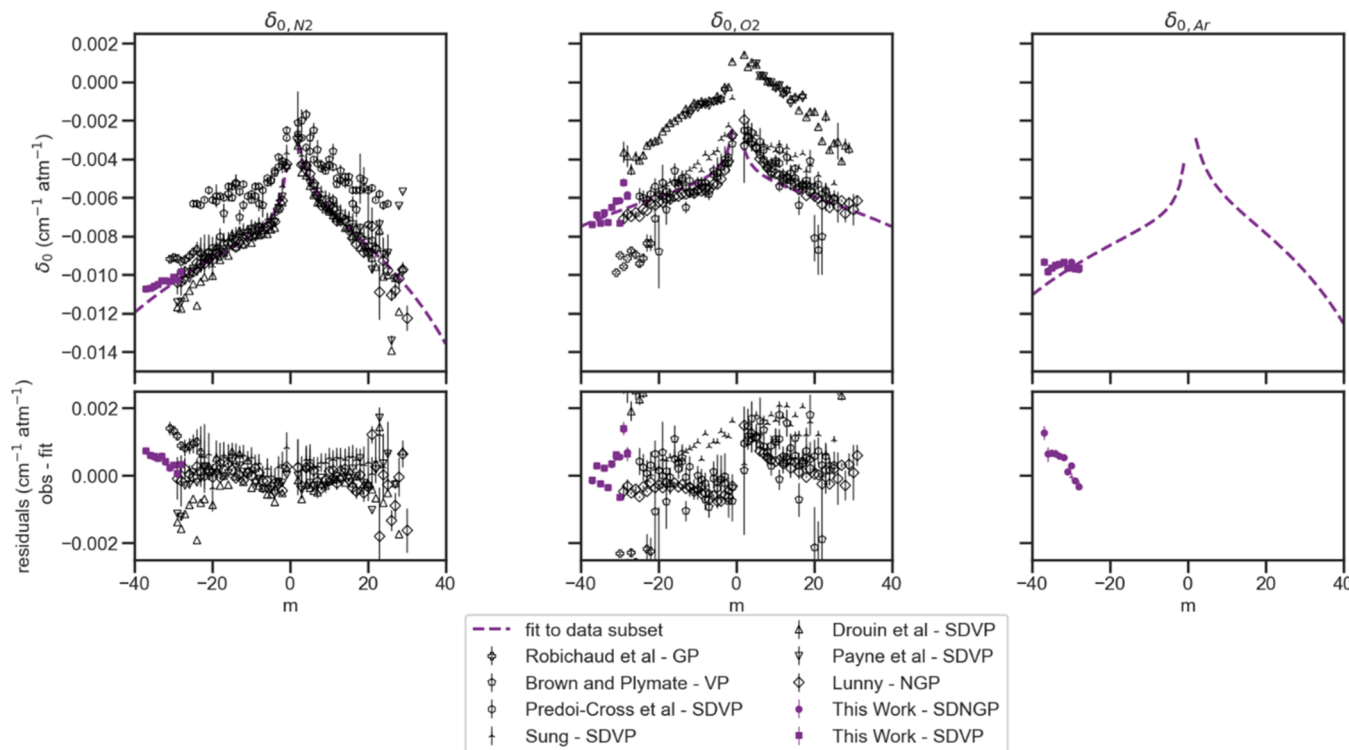


Fig. 3. Comparison of N₂, O₂, and Ar pressure shifting coefficients reported here and in the literature. Error bars represent the combined standard uncertainty in the fitted parameters for the current measurements and reported uncertainties for literature values.

approximant functions to the literature and present measurements. This analysis was identical to that carried out for pressure broadening data, except that the data were not weighted. The resulting empirical model

for the N₂ pressure shift included the data from Robichaud et al. [14], Drouin et al. [18], Payne et al. [19], Lunny [22], and Sung [23], which agreed well with the current measurements. The fit to the O₂ pressure

shifts included the data of Lunny [22], Brown and Plymate [11], Predoi-Cross et al. [12,13], and Sung [23]. The residuals of the data included in the fits with respect to the empirical models had a standard deviation of 8.3 % for δ_{0,N_2} and 15.9 % for δ_{0,O_2} . To our knowledge, this work is the first to report Ar pressure shifts in the O₂ A-band. Therefore, to extrapolate our high J measurements of $\delta_{0,Ar}$ to lower- J values, we estimate $\delta_{0,Ar}(m)$ to be $\delta_{0,N_2}(m) \langle \delta_{0,Ar} / \delta_{0,N_2} \rangle$, where $\langle \delta_{0,Ar} / \delta_{0,N_2} \rangle = 0.923$ is based on the high J measurements reported here. Because $\delta_{0,Ar}$ is similar in magnitude to that of δ_{0,N_2} , adverse impacts on atmospheric retrievals caused by neglecting Ar (either by explicitly assuming $\delta_{0,Ar} = \delta_{0,N_2}$ or by using a synthetic air sample) pressure shifting should be less significant than those associated with the neglect of pressure broadening caused by Ar. However, the literature discrepancy in O₂ pressure shifts, and to a lesser extent, N₂ pressure shifts, indicates the need for additional investigation as this could lead to biases in atmospheric retrievals.

In Fig. 4, we compare the speed dependent and Dicke narrowing parameters, $a_{w,air}$ and $\tilde{\nu}_{VC,air}$, respectively, reported here and in the literature. There are no literature values for Dicke narrowing based on a hard collision model, but Robichaud et al. [14], Havey et al. [15], and Long et al. [16] report values determined with a line profile using the soft collision model, GP. The $\tilde{\nu}_{VC,air}$ values reported in this work were determined using the SDNGP, which uses a hard collision model and accounts for both speed dependent narrowing and Dicke narrowing. Because accounting for only one narrowing mechanism will tend to bias the Dicke narrowing high [49], our inclusion of an additional narrowing mechanism explains our lower $\tilde{\nu}_{VC,air}$ values compared to those in Robichaud et al. [14], Havey et al. [15], and Long et al. [16]. Over the studied range of transitions, our measurements did not show the decrease in $\tilde{\nu}_{VC,air}$ with decreasing J as previously reported in the literature. However, this could be due to the limited number of lines included in the study. In our reported $a_{w,air}$ values, we observe the same effect where the $a_{w,air}$ value obtained by fitting with the SDVP is larger than that obtained with the SDNGP. In Drouin et al. [18] and Payne et al. [19], $a_{w,air}$ values for most of the high J transitions measured in this study were fixed in their fits and are therefore not included in Fig. 4. However, in the present work the resulting SDVP $a_{w,air}$ values follow a J -dependent trend qualitatively similar to those reported by Drouin et al. [18] and Payne et al. [19].

3.2. Atmospheric implications

Because Ar constitutes only 0.934 % of atmospheric air by volume, even significant changes in Ar spectroscopic parameters result in only small perturbations of the air-broadening parameters. However, estimating the sensitivity of atmospheric retrievals to small changes in the spectroscopic parameters can be difficult in partially saturated bands

like the O₂ A-band, where effects can be nonlinear. We investigated the magnitude of the impact of this perturbation on atmospheric measurements in two ways. First, we performed a surface pressure retrieval sensitivity study on synthetic atmospheric spectra simulated with a whole-air (containing Ar) line list and evaluated with a synthetic-air line list (not containing Ar). Second, we compared retrievals of O₂ total column for actual atmospheric spectra collected at the Total Carbon Column Observing Network (TCCON) station located at Park Falls, WI, USA [58].

Using the empirical models described above (available in the Supplementary Materials), we model the collisional broadening and shifting parameters for O₂, N₂, and Ar. For each line in the band ($J' \leq 45$), we calculate synthetic-air and whole-air collisional broadening and shifting terms, defining synthetic-air and whole-air as in Table 1. The line lists for the synthetic spectra sensitivity study used the SDVP HITRAN 2020 O₂ A-band line list based on Payne et al., updating the collision broadening and shifting terms for the tested line lists [19,57]. The whole- and synthetic-air line lists for the TCCON tests updated the collisional broadening and shifting terms in the VP based TCCON telluric line list. We also updated the line intensities to those reported in Adkins et al. [42].

For the surface pressure sensitivity study, we simulate atmospheric spectra using TCCON priors for temperature and pressure as a function of altitude averaged by available month and time information for each TCCON site (32 sites) [1,59]. This set comprises 1580 simulations covering various locations, months, and times of day, providing sampling over a range of airmasses. An atmospheric spectrum is simulated as the sum of altitudinal atmospheric slices based on the TCCON priors (pressure, temperature, and slice thickness). The spectra were simulated with a signal-to-noise ratio of 1000. We also used a Gaussian filter with a width of 0.05 cm⁻¹ when both simulating with the whole-air line list and fitting with the synthetic-air line list. The relative pressure profile across the simulated atmospheric column was conserved, and only the surface pressure was fit to minimize the residuals.

Fig. 5 shows the surface pressure bias in atmospheric spectra obtained by simulating with a whole-air line list and fitting with a synthetic-air line list. Using the latter list in the analysis results in a systematic underprediction of retrieved surface pressure. The average surface pressure bias across all simulated airmasses is -0.69 ± 0.05 hPa, in comparison to the simulated average surface pressure of 1016.5 hPa. Bias is defined here as the difference between the fitted and the simulated surface pressure. Additionally, there is a slight airmass dependence, with larger airmass increasing the magnitude of the bias. In comparison, the average global surface pressure bias between the OCO-2 retrieval and its prior meteorology is about 2.5 hPa [19] and opposite in sign.

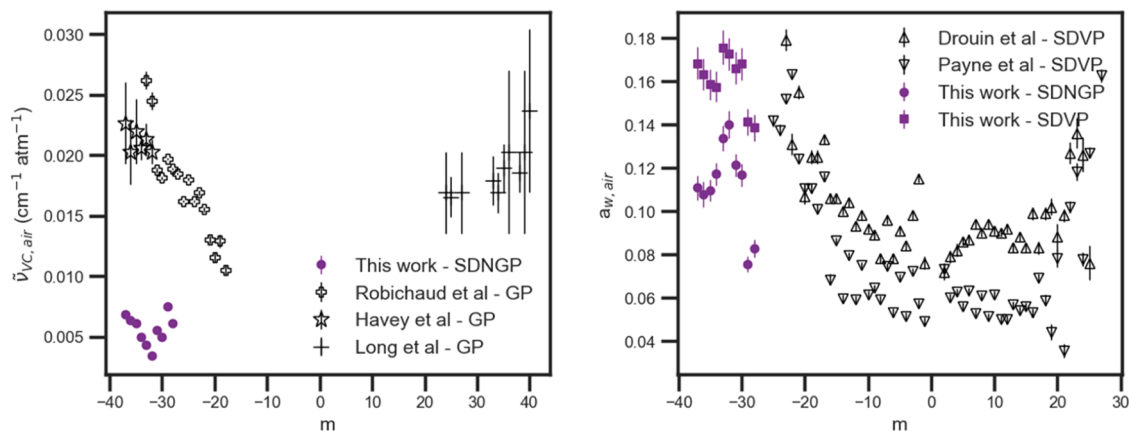


Fig. 4. Comparison of the Dicke narrowing (left) and speed-dependence (right) air-broadened parameters reported here and in the literature. Error bars represent the combined standard uncertainty in the fitted parameters for the current measurements and reported uncertainties for literature values.

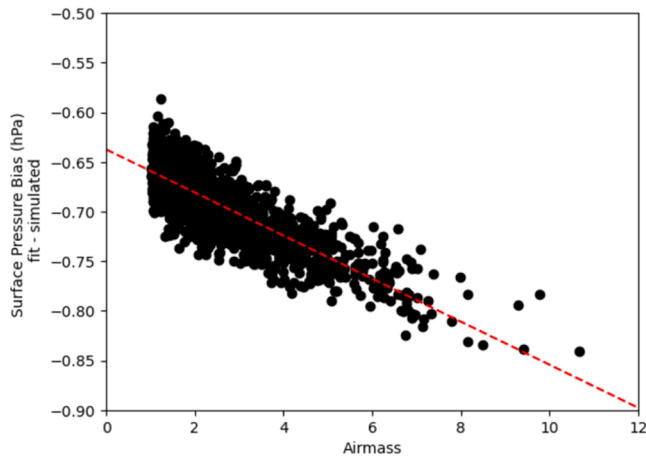


Fig. 5. Results of surface pressure bias in simulated atmospheric spectra simulated with a whole-air line list (including Ar) and fit with a synthetic-air line list (excluding Ar). The latter list underpredicts the surface pressure, increasing the magnitude of the bias at larger airmasses. The linear fit (red line) has a slope of $-0.02169(6)$ hPa/airmass and an intercept of $-0.637(2)$ hPa.

As a second test of the atmospheric impacts of neglecting Ar contributions to air-broadened line-shape parameters, we compare retrievals of O_2 total columns from the TCCON station located at Park Falls, WI, USA [58]. To replicate the results of the simulation shown in Fig. 5, we computed surface pressure from the retrieved O_2 A-band and H_2O columns using

$$p = \frac{v_{O_2}}{f_{O_2}} M_{air, dry} \bar{g} + v_{H_2O} M_{H_2O} \bar{g} \quad (3)$$

where v_{O_2} and v_{H_2O} are the total columns of O_2 and H_2O , respectively, retrieved using the GGG2020 algorithm [59] with the synthetic-air and whole-air line lists, f_{O_2} is the mean atmospheric amount fraction of O_2 (calculated as 0.209294 for the year 2024 following appendix E2 of Ref. [59]), $M_{air, dry}$ and M_{H_2O} are the molar masses of dry air ($28.964 \text{ g mol}^{-1}$) and H_2O ($18.01534 \text{ g mol}^{-1}$), respectively, and \bar{g} is the mean gravitational acceleration over the total column (for which we used 9.784 m s^{-2}), calculated as a pressure-weighted mean value for the TCCON observations used in this test.

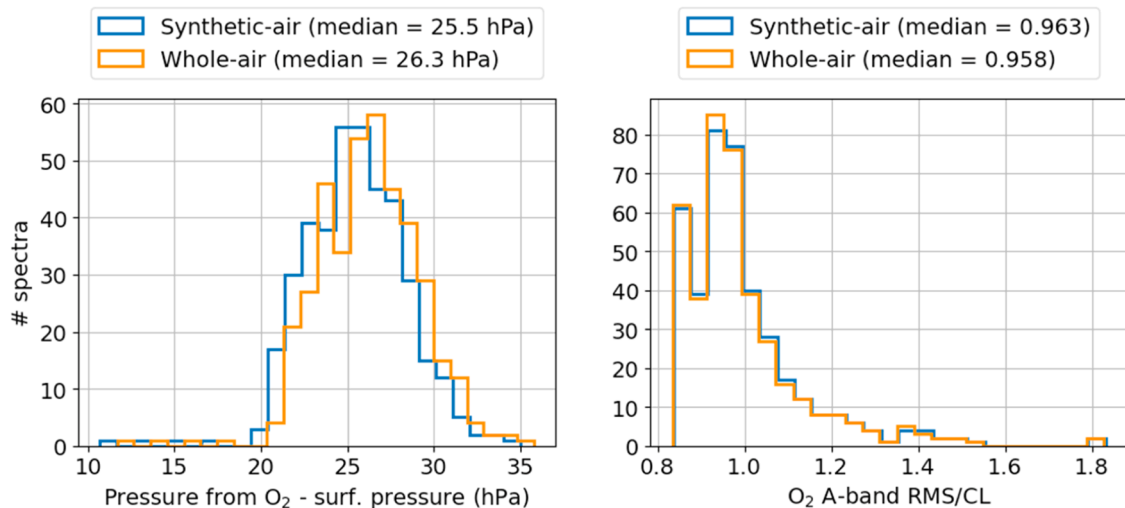


Fig. 6. Analysis of whole- and synthetic-air line lists in the TCCON A-band window for 397 spectra recorded at the Park Falls, WI, USA TCCON station (168 spectra from 2 Feb 2024 and 229 spectra from 1 Jul 2024). Left panel: Difference between surface pressure calculated from the O_2 columns using Eq. (3) and the measured surface pressure at the Park Fall TCCON station. Right panel: Histograms of the root-mean-squared residual in the TCCON O_2 A-band retrieval window ($12,970 \text{ cm}^{-1}$ to $13,195 \text{ cm}^{-1}$) normalized by the continuum level of the spectrum.

The left panel of Fig. 6 shows histograms of the difference in surface pressure calculated from Eq. (3) versus the measured surface pressure at the Park Falls TCCON site for GGG2020 retrievals, on two days of Park Falls TCCON spectra (one in the winter and one in the summer) using the synthetic-air and whole-air line lists. Consistent with Fig. 5, the whole-air line list leads to a greater retrieved surface pressure than the synthetic air-line list. The synthetic-air line list results in a median difference in retrieved surface pressure from measured surface pressure that is 0.8 hPa smaller than the whole-air line list, which is consistent with the -0.69 ± 0.05 hPa result from the sensitivity tests. Both line lists show an overall positive bias in surface pressure, which could be due to the lack of self-consistency in the line list construction (i.e., differences in line profile, differences in line centers). Note that TCCON does not use the A-band in their standard retrievals; instead, they use the O_2 band centered at $1.27 \mu\text{m}$ to retrieve O_2 because it is advantageous to retrieve O_2 , CO_2 , CH_4 , and other target gases from spectral windows recorded by the same detector [1].

While the comparison to surface pressure is unclear as to which line list yields a more accurate surface pressure due to the mean bias, the spectral residuals from the TCCON analysis show that the whole-air line list leads to slightly improved spectral fits. The right panel of Fig. 6 shows the distribution of root-mean-squared residuals (normalized by the continuum level) for retrievals of the same set of Park Falls spectra as in the previous paragraph. The whole-air line list has slightly smaller residuals overall (quantified by the median results), indicating a better fit to the observed solar spectra when Ar-broadening is included in the air collisional broadening and pressure shifting terms.

These analyses suggest that while atmospheric retrieval biases due to O_2 A-band spectroscopy are still dominated by uncertainty in the higher-order line-shape parameters, line-mixing, and collision-induced absorption models [17], the use of line lists that neglect the contributions of Ar to the collisional broadening and shifting introduces a non-negligible error in O_2 A-band surface pressure retrievals. Including the line-shape effects of Ar in future analyses would reduce this bias. The consistency in surface pressure impact between the simulation-based sensitivity analysis and the TCCON retrieval analysis indicates that sensitivity tests on synthetic spectra are a valid tool for testing impacts of deficiencies in subsets of the total spectroscopic model, which might be confounded by the complexities of full atmospheric retrievals.

4. Conclusions

In this work, we report pressure broadening and shifting parameters for O₂, N₂, and Ar for ten high *J* lines in the P-branch of the O₂ A-band. Consistent with prior measurements, pressure broadening by Ar is smaller than that of O₂ or N₂, while pressure shifting by Ar is larger than that of N₂ and smaller than that of O₂. Additionally, we have compiled literature data and current measurements to report empirical models of O₂, N₂, and Ar collisional broadening and pressure shifting in the O₂ A-band. The empirical models presented herein, incorporating both the present data and literature results, should also be useful for calculating the room-temperature broadening and shifting line-shape parameters in the O₂ A-band for whole-air and arbitrary mixtures comprising N₂, O₂, and Ar.

These empirical models highlight the current levels of literature consensus in air-component collisional broadening and pressure shifting terms. There is literature agreement at the ~5 % level for O₂ and N₂ collisional broadening parameters. In contrast, the O₂ and N₂ pressure shifting parameters have larger systematic disagreements between various literature data sets. This indicates the need for additional studies focusing on pressure shifts in the O₂ A-band, specifically the self-shifts.

For most atmospheric measurements, neglecting Ar line parameter contributions likely leads to only a small offset in the retrieved surface pressure values. The initial simulations and TCCON retrievals in this work show that the impact is about 0.75 hPa in magnitude (0.07 %) – within a factor of four of the OCO-2 target uncertainty of 0.25 % for CO₂ amount fraction. However, newer missions like the CO₂ monitoring mission within the European Union's Copernicus Program (CO2M) have more rigorous precision targets (~0.15 %), requiring reduction of every possible source of error in retrievals [60]. As available spectroscopic parameters and atmospheric measurements continue to improve, the line-shape effects of Ar should be considered. The empirical models for Ar collisional broadening and pressure shifting presented in this work provide a first step towards the incorporation of Ar line parameters in O₂ A-band line lists. Future high-resolution and high-precision laboratory measurements of air-broadening can be made using air samples containing Ar to easily consider whole-air line-shape effects. If attainable, researchers should also report air-component line-shape parameters because this allows for the use of line-shape parameters for both synthetic-air and whole-air applications.

CRedit authorship contribution statement

Leah E. Stevenson: Writing – review & editing, Writing – original draft, Visualization, Investigation, Formal analysis. **Joshua L. Laughner:** Formal analysis, Visualization, Writing – original draft. **Mitchio Okumura:** Writing – review & editing, Supervision, Project administration, Funding acquisition. **Joseph T. Hodges:** Writing – review & editing, Supervision, Project administration, Funding acquisition. **Erin M. Adkins:** Writing – review & editing, Writing – original draft, Visualization, Supervision, Methodology, Investigation, Formal analysis, Data curation, Conceptualization.

Declaration of competing interest

The authors declare that they have no known competing financial interests or personal relationships that could have appeared to influence the work reported in this paper.

Acknowledgments

EMA and JTH acknowledge funding from the NIST Greenhouse Gas and Climate Science Program and the National Aeronautics and Space Administration (NASA) [contract NNH20ZDA0001N–OCOT(NIST)]. LES acknowledges support of a National Science Foundation Graduate Research Fellowship under Grant No 2139433. Work at Caltech (MO and

LES) was funded by NASA Grant Numbers 80NSSC21K1331 and 80NSSC24K0746. A portion of this research was carried out at the Jet Propulsion Laboratory (JPL), California Institute of Technology, under a contract with NASA (80NM0018D0004). Government sponsorship is acknowledged. JLL and the operation of the Park Falls TCCON site were supported by NASA funding through grant 80NSSC22K1066. The authors would like to thank Adam J. Fleisher (NIST) and Sean M. Bresler (NIST) for commenting on the manuscript.

Supplementary materials

Supplementary material associated with this article can be found, in the online version, at doi:10.1016/j.jqsrt.2025.109480.

Data availability

Data will be available on request and at <https://data.nist.gov>.

References

- [1] Wunch D, Toon GC, Blavier J-FL, Washenfelder RA, Notholt J, Connor BJ, et al. The total carbon column observing network. *Philos Trans R Soc Math Phys Eng Sci* 2011;369:2087–112. <https://doi.org/10.1098/rsta.2010.0240>.
- [2] Oshchepkov S, Bril A, Maksyutov S, Yokota T. Detection of optical path in spectroscopic space-based observations of greenhouse gases: application to GOSAT data processing. *J Geophys Res* 2011;116. <https://doi.org/10.1029/2010JD015352>. D14304.
- [3] Crisp D, Pollock HR, Rosenberg R, Chapsky L, Lee RAM, Oyafuso FA, et al. The on-orbit performance of the Orbiting Carbon Observatory-2 (OCO-2) instrument and its radiometrically calibrated products. *Atmospheric Meas Tech* 2017;10:59–81. <https://doi.org/10.5194/amt-10-59-2017>.
- [4] Eldering A, Taylor TE, O'Dell CW, Pavlick R. The OCO-3 mission: measurement objectives and expected performance based on 1 year of simulated data. *Atmospheric Meas Tech* 2019;12:2341–70. <https://doi.org/10.5194/amt-12-2341-2019>.
- [5] Liu Y, Wang J, Yao L, Chen X, Cai Z, Yang D, et al. The TanSat mission: preliminary global observations. *Sci Bull* 2018;63:1200–7. <https://doi.org/10.1016/j.scib.2018.08.004>.
- [6] Barton IJ, Scott JC. Remote measurement of surface pressure using absorption in the oxygen A-band. *Appl Opt* 1986;25:3502. <https://doi.org/10.1364/AO.25.003502>.
- [7] Geddes A, Bösch H. Tropospheric aerosol profile information from high-resolution oxygen A-band measurements from space. *Atmospheric Meas Tech* 2015;8:859–74. <https://doi.org/10.5194/amt-8-859-2015>.
- [8] Fischer J, Grassl H. Detection of cloud-top height from backscattered radiances within the oxygen A band. Part 1: theoretical study. *J Appl Meteorol* 1991;30:1245–59. [https://doi.org/10.1175/1520-0450\(1991\)030<1245:DOCTHF>2.0.CO;2](https://doi.org/10.1175/1520-0450(1991)030<1245:DOCTHF>2.0.CO;2).
- [9] Koелеmeijer RBA, Stammes P, Hovenier JW, De Haan JF. A fast method for retrieval of cloud parameters using oxygen A band measurements from the Global Ozone Monitoring Experiment. *J Geophys Res Atmospheres* 2001;106:3475–90. <https://doi.org/10.1029/2000JD900657>.
- [10] Frankenberg C, Pollock R, Lee RAM, Rosenberg R, Blavier J-F, Crisp D, et al. The Orbiting Carbon Observatory (OCO-2): spectrometer performance evaluation using pre-launch direct sun measurements. *Atmospheric Meas Tech* 2015;8:301–13. <https://doi.org/10.5194/amt-8-301-2015>.
- [11] Brown LR, Plymate C. Experimental line parameters of the oxygen A band at 760 nm. *J Mol Spectrosc* 2000;199:166–79. <https://doi.org/10.1006/jmsp.1999.8012>.
- [12] Predoi-Cross A, Holladay C, Heung H, Bouanich J-P, GCh Mellau, Keller R, et al. Nitrogen-broadened lineshapes in the oxygen A-band: experimental results and theoretical calculations. *J Mol Spectrosc* 2008;251:159–75. <https://doi.org/10.1016/j.jms.2008.02.010>.
- [13] Predoi-Cross A, Hambrook K, Keller R, Povey C, Schofield I, Hurtmans D, et al. Spectroscopic lineshape study of the self-perturbed oxygen A-band. *J Mol Spectrosc* 2008;248:85–110. <https://doi.org/10.1016/j.jms.2007.11.007>.
- [14] Robichaud DJ, Hodges JT, Brown LR, Lisak D, Maslowski P, Yeung LY, et al. Experimental intensity and lineshape parameters of the oxygen A-band using frequency-stabilized cavity ring-down spectroscopy. *J Mol Spectrosc* 2008;248:1–13. <https://doi.org/10.1016/j.jms.2007.10.010>.
- [15] Havey DK, Long DA, Okumura M, Miller CE, Hodges JT. Ultra-sensitive optical measurements of high-*J* transitions in the O₂ A-band. *Chem Phys Lett* 2009;483:49–54. <https://doi.org/10.1016/j.cplett.2009.10.067>.
- [16] Long DA, Havey DK, Okumura M, Miller CE, Hodges JT. O₂ A-band line parameters to support atmospheric remote sensing. *J Quant Spectrosc Radiat Transf* 2010;111:2021–36. <https://doi.org/10.1016/j.jqsrt.2010.05.011>.
- [17] Long DA, Hodges JT. On spectroscopic models of the O₂ A-band and their impact upon atmospheric retrievals. *J Geophys Res Atmospheres* 2012;117. <https://doi.org/10.1029/2012JD017807>. n/a-n/a.

- [18] Drouin BJ, Benner DC, Brown LR, Cich MJ, Crawford TJ, Devi VM, et al. Multispectrum analysis of the oxygen A-band. *J Quant Spectrosc Radiat Transf* 2017;186:118–38. <https://doi.org/10.1016/j.jqsrt.2016.03.037>.
- [19] Payne VH, Drouin BJ, Oyafuso F, Kuai L, Fisher BM, Sung K, et al. Absorption coefficient (ABSCO) tables for the Orbiting Carbon Observatories: version 5.1. *J Quant Spectrosc Radiat Transf* 2020;255:107217. <https://doi.org/10.1016/j.jqsrt.2020.107217>.
- [20] Tran H, Boulet C, Hartmann J-M. Line mixing and collision-induced absorption by oxygen in the A band: laboratory measurements, model, and tools for atmospheric spectra computations. *J Geophys Res* 2006;111. <https://doi.org/10.1029/2005JD006869>. D15210.
- [21] Karman T, Koenis MAJ, Banerjee A, Parker DH, Gordon IE, van der Avoird A, et al. O₂–O₂ and O₂–N₂ collision-induced absorption mechanisms unravelled. *Nat Chem* 2018;10:549–54. <https://doi.org/10.1038/s41557-018-0015-x>.
- [22] Lunny EM. High-Resolution photoacoustic spectroscopy of the oxygen A-Band. California Institute of Technology; 2020. <https://doi.org/10.7907/QXCM-4909>.
- [23] Sung K. O₂ (A) band updates simultaneous determination of line mixing and. CIA 2024.
- [24] Connor B, Bösch H, McDuffie J, Taylor T, Fu D, Frankenberg C, et al. Quantification of uncertainties in OCO-2 measurements of XCO₂: simulations and linear error analysis. *Atmospheric Meas Tech* 2016;9:5227–38. <https://doi.org/10.5194/amt-9-5227-2016>.
- [25] Hobbs JM, Drouin BJ, Oyafuso F, Payne VH, Gunson MR, McDuffie J, et al. Spectroscopic uncertainty impacts on OCO-2/3 retrievals of XCO₂. *J Quant Spectrosc Radiat Transf* 2020;257:107360. <https://doi.org/10.1016/j.jqsrt.2020.107360>.
- [26] Schubert G, Walterscheid RL. Earth. editor. In: Cox AN, editor. *Allen's astrophys. quant.* New York, NY: Springer New York; 2002. p. 239–92. <https://doi.org/10.1007/978-1-4612-1186-0-11>.
- [27] Tan Y, Kochanov RV, Rothman LS, Gordon IE. Introduction of water-vapor broadening parameters and their temperature-dependent exponents into the HITRAN database: part I—CO₂, N₂O, CO, CH₄, O₂, NH₃, and H₂S. *J Geophys Res Atmospheres* 2019;124:11580–94. <https://doi.org/10.1029/2019JD030929>.
- [28] Vess EM, Wallace CJ, Campbell HM, Awadalla VE, Hodges JT, Long DA, et al. Measurement of H₂O broadening of O₂ A-band transitions and implications for atmospheric remote sensing. *J Phys Chem A* 2012;116:4069–73. <https://doi.org/10.1021/jp301194j>.
- [29] Drouin BJ, Payne V, Oyafuso F, Sung K, Mlawer E. Pressure broadening of oxygen by water. *J Quant Spectrosc Radiat Transf* 2014;133:190–8. <https://doi.org/10.1016/j.jqsrt.2013.08.001>.
- [30] Pope RS, Wolf PJ, Perram GP. A study of collision broadening in the O₂ A-band with the noble gases using fourier transform spectroscopy. *J Mol Spectrosc* 2004;223:205–13. <https://doi.org/10.1016/j.jms.2003.12.004>.
- [31] Pope RS, Wolf PJ, Perram GP. Collision broadening of rotational transitions in the O₂A band by molecular perturbers. *J Quant Spectrosc Radiat Transf* 2000;64:363–77. [https://doi.org/10.1016/S0022-4073\(99\)00109-0](https://doi.org/10.1016/S0022-4073(99)00109-0).
- [32] Klemm J, Campargue A, Fleurbaey H, Kassl S, Romanini D, Mondelain D. Temperature dependence of the air-broadened line-shape parameters of the 1.27 μm O₂-band. *J Quant Spectrosc Radiat Transf* 2025. Under review.
- [33] Malathy Devi V, Benner DC, Miller CE, Predoi-Cross A. Lorentz half-width, pressure-induced shift and speed-dependent coefficients in oxygen-broadened CO₂ bands at 6227 and 6348 cm⁻¹ using a constrained multispectrum analysis. *J Quant Spectrosc Radiat Transf* 2010;111:2355–69. <https://doi.org/10.1016/j.jqsrt.2010.06.003>.
- [34] Adkins EM, Long DA, Hodges JT. Air-broadening in near-infrared carbon dioxide line shapes: quantifying contributions from O₂, N₂, and Ar. *J Quant Spectrosc Radiat Transf* 2021;270:107669. <https://doi.org/10.1016/j.jqsrt.2021.107669>.
- [35] Nara H, Tanimoto H, Tohjima Y, Mukai H, Nojiri Y, Katsumata K, et al. Effect of air composition (N₂, O₂, Ar, and H₂O) on CO₂ and CH₄ measurement by wavelength-scanned cavity ring-down spectroscopy: calibration and measurement strategy. *Atmospheric Meas Tech* 2012;5:2689–701. <https://doi.org/10.5194/amt-5-2689-2012>.
- [36] Long DA, Gameson L, Truong G-W, Bielska K, Cygan A, Hodges JT, et al. The effects of variations in buffer gas mixing ratios on commercial carbon dioxide cavity ring-down spectroscopy sensors. *J Atmospheric Ocean Technol* 2013;30:2604–9. <https://doi.org/10.1175/JTECH-D-13-00039.1>.
- [37] Brewer PJ, Brown RJC, Miller MN, Miñarro MD, Murugan A, Milton MJT, et al. Preparation and validation of fully synthetic standard gas mixtures with atmospheric isotopic composition for global CO₂ and CH₄ monitoring. *Anal Chem* 2014;86:1887–93. <https://doi.org/10.1021/ac403982m>.
- [38] Kelley ME, Rhoderick GC, Guenther FR. Development and verification of air balance gas primary standards for the measurement of nitrous oxide at atmospheric levels. *Anal Chem* 2014;86:4544–9. <https://doi.org/10.1021/ac500581b>.
- [39] Johnson JE, Rella CW. Effects of variation in background mixing ratios of N₂, O₂, and Ar on the measurement of δ¹⁸O–H₂O and δ²H–H₂O values by cavity ring-down spectroscopy. *Atmospheric Meas Tech* 2017;10:3073–91. <https://doi.org/10.5194/amt-10-3073-2017>.
- [40] Truong G-W, KO Douglass, Maxwell SE, Van Zee RD, Plusquellic DF, Hodges JT, et al. Frequency-agile, rapid scanning spectroscopy. *Nat Photonics* 2013;7:532–4. <https://doi.org/10.1038/nphoton.2013.98>.
- [41] Lin H, Reed ZD, Sironneau VT, Hodges JT. Cavity ring-down spectrometer for high-fidelity molecular absorption measurements. *J Quant Spectrosc Radiat Transf* 2015;161:11–20. <https://doi.org/10.1016/j.jqsrt.2015.03.026>.
- [42] Adkins EM, Yurchenko S, Somogyi W, Tennyson J, Hodges JT. An accurate determination of O₂ A-band line intensities through experiment and theory. *J Quant Spectrosc Radiat Transf* 2025.
- [43] Adkins E. Multi-spectrum analysis tool for spectroscopy (MATS) 2020. <https://doi.org/10.18434/M32200>.
- [44] Fleisher AJ, Adkins EM, Reed ZD, Yi H, Long DA, Fleurbaey HM, et al. Twenty-five-fold reduction in measurement uncertainty for a molecular line intensity. *Phys Rev Lett* 2019;123. <https://doi.org/10.1103/PhysRevLett.123.043001>. 043001.
- [45] Hodges JT, Laver HP, Miller WW, Scace GE. Frequency-stabilized single-mode cavity ring-down apparatus for high-resolution absorption spectroscopy. *Rev Sci Instrum* 2004;75:849–63. <https://doi.org/10.1063/1.1666984>.
- [46] Zhang J, Lu ZH, Wang LJ. Precision refractive index measurements of air, N₂, O₂, Ar, and CO₂ with a frequency comb. *Appl Opt* 2008;47:3143. <https://doi.org/10.1364/AO.47.003143>.
- [47] Rhoderick GC, Kelley ME, Miller WR, Brailsford G, Possolo A. Development of a southern oceanic air standard reference material. *Anal Bioanal Chem* 2016;408:1159–69. <https://doi.org/10.1007/s00216-015-9218-9>.
- [48] Hanson E, Olson DA, Liu H, Ahmed Z, KO Douglass. Towards traceable transient pressure metrology. *Metrologia* 2018;55:275–83. <https://doi.org/10.1088/1681-7575/aaad1b>.
- [49] Adkins EM, Hodges JT. Assessment of the precision, bias and numerical correlation of fitted parameters obtained by multi-spectrum fits of the Hartmann-Tran line profile to simulated absorption spectra. *J Quant Spectrosc Radiat Transf* 2022;280:108100. <https://doi.org/10.1016/j.jqsrt.2022.108100>.
- [50] Kochanov RV, Gordon IE, Rothman LS, Wcislo P, Hill C, Wilzewski JS. HITRAN Application Programming Interface (HAPI): a comprehensive approach to working with spectroscopic data. *J Quant Spectrosc Radiat Transf* 2016;177:15–30. <https://doi.org/10.1016/j.jqsrt.2016.03.005>.
- [51] Ngo NH, Lisak D, Tran H, Hartmann J-M. An isolated line-shape model to go beyond the Voigt profile in spectroscopic databases and radiative transfer codes. *J Quant Spectrosc Radiat Transf* 2013;129:89–100. <https://doi.org/10.1016/j.jqsrt.2013.05.034>.
- [52] Tennyson J, Bernath PF, Campargue A, Császár AG, Daumont L, Gamache RR, et al. Recommended isolated-line profile for representing high-resolution spectroscopic transitions (IUPAC Technical Report). *Pure Appl Chem* 2014;86:1931–43. <https://doi.org/10.1515/pac-2014-0208>.
- [53] Rosenkranz P. Shape of the 5 mm oxygen band in the atmosphere. *IEEE Trans Antennas Propag* 1975;23:498–506. <https://doi.org/10.1109/TAP.1975.1141119>.
- [54] Wcislo P, Gordon IE, Tran H, Tan Y, Hu S-M, Campargue A, et al. The implementation of non-Voigt line profiles in the HITRAN database: H₂ case study. *J Quant Spectrosc Radiat Transf* 2016;177:75–91. <https://doi.org/10.1016/j.jqsrt.2016.01.024>.
- [55] Joint Committee for Guides in Metrology. Evaluation of measurement data—Guide to the expression of uncertainty in measurement. *JCGM* 2008;100:1–116. <https://doi.org/10.59161/JCGM100-2008E>.
- [56] Fleurbaey H, Reed ZD, Adkins EM, Long DA, Hodges JT. High accuracy spectroscopic parameters of the 1.27 μm band of O₂ measured with comb-referenced, cavity ring-down spectroscopy. *J Quant Spectrosc Radiat Transf* 2021;270:107684. <https://doi.org/10.1016/j.jqsrt.2021.107684>.
- [57] Gordon IE, Rothman LS, Hargreaves RJ, Hashemi R, Karlovets EV, Skinner FM, et al. The HITRAN2020 molecular spectroscopic database. *J Quant Spectrosc Radiat Transf* 2022;277:107949. <https://doi.org/10.1016/j.jqsrt.2021.107949>.
- [58] Washenfelder RA, Toon GC, Blavier J-F, Yang Z, Allen NT, Wennberg PO, et al. Carbon dioxide column abundances at the Wisconsin Tall Tower site. *J Geophys Res Atmospheres* 2006;111. <https://doi.org/10.1029/2006JD007154>. 2006JD007154.
- [59] Laughner JL, Toon GC, Mendonca J, Petri C, Roche S, Wunch D, et al. The total carbon column observing network's GGG2020 data version. *Earth Syst Sci Data* 2024;16:2197–260. <https://doi.org/10.5194/essd-16-2197-2024>.
- [60] Yasjka M, Boesch H, Bombelli A, Brunner D, Buchwitz M, Ciais P, et al. Copernicus CO₂ monitoring mission requirements document. European Space Agency; 2020.